MITSUBISHI ELECTRIC RESEARCH LABORATORIES
https://www.merl.com

Harmonic Signature Extraction in Motor Fault Detection via a Weighted Sparsity-driven and Graph-based Model

Shinya, Tsurutashin; Liu, Dehong

TR2024-067 June 11, 2024

Abstract

Harmonics are important signatures in motor current indicating motor operating conditions and faults in motor maintenance. However, harmonics of motor faults are generally very weak and with frequency-dependent magnitudes, making it difficult to extract harmonics from noisy measurements, especially when the motor speed is varying. This paper introduces a novel weighted sparsity-driven and graph-model-based method to extract harmonics in the time-frequency domain. The method utilizes sparsity of harmonics in the frequency domain and their smoothness in the time domain due speed variation, and uses a frequency-dependent weight to leverage the magnitude of different harmonics. We formulate the harmonic signature extraction as a regularized optimization problem, and solve it us an alternating direction method of multipliers (ADMM). Results on experimental data show that the proposed method can effectively extract weak harmonic components in noisy measurements with improved performance over other existing methods.

The IFAC Safeprocess 2024 Symposium

Mitsubishi Electric Research Laboratories, Inc.
201 Broadway, Cambridge, Massachusetts 02139

Harmonic Signature Extraction in Motor Fault Detection via a Weighted Sparsity-driven and Graph-based Model

Shinya Tsuruta [*,**] **Dehong Liu** [*]

[*] *Mitsubishi Electric Research Laboratories, Cambridge, MA, 02139, USA (e-mail: {tsuruta, liudh}@merl.com).*
[**] *Information Technology R&D Center, Mitsubishi Electric Corporation, Ofuna, Yokohama 247-8501 Japan (e-mail: Tsuruta.Shinya@dw.MitsubishiElectric.co.jp).*

Abstract: Harmonics are important signatures in motor current indicating motor operating conditions and faults in motor maintenance. However, harmonics of motor faults are generally very weak and with frequency-dependent magnitudes, making it difficult to extract harmonics from noisy measurements, especially when the motor speed is varying. This paper introduces a novel weighted sparsity-driven and graph-model-based method to extract harmonics in the time-frequency domain. The method utilizes sparsity of harmonics in the frequency domain and their smoothness in the time domain due speed variation, and uses a frequency-dependent weight to leverage the magnitude of different harmonics. We formulate the harmonic signature extraction as a regularized optimization problem, and solve it us an alternating direction method of multipliers (ADMM). Results on experimental data show that the proposed method can effectively extract weak harmonic components in noisy measurements with improved performance over other existing methods.

Keywords: Fault detection, sparsity, smooth signal, graph model

1. INTRODUCTION

Induction motors are important drive machines for industries because they are cost-effective, robust, and endurable for different environmental conditions. As induction motors are widely used in mining, cement, automotive, oil and gas, and manufacturing industries, preventive maintenance of induction motors also receives increasing attentions.

In recent decades, motor current signature analysis(MCSA) (Pillay and Xu (1996)) has been used to detect motor faults for its non-invasive property. When a motor fault occurs, the rotating magnetic field becomes asymmetric, inducing extra frequency components as fault signatures in the stator current. MCSA-based methods aim to extract fault signatures that indicate abnormalities.

One type of fault signature is side-band frequencies around the supply frequency, such as broken-bar fault signature and eccentricity fault(Thomson and Fenger (2001)). However, side-band fault signatures, such as broken-bar fault signature, may be difficult to extract because their small magnitudes and proximity to the supply frequency, especially when the slip of motor speed is very small.

Another type of fault signature is harmonics in a relatively higher frequency band, such as slot harmonics. When rotor bars cross the magnetic field generated by the stator windings, slot harmonics are generated in the stator current (Vas (1992)). Since slot harmonics are affected by the air gap between the stator and rotor and the speed of the rotor, they can be used for eccentricity detection(Faiz and Moosavi (2016)), in-turn fault defects(Bonet-Jara et al. (2022)), and sensorless speed control(Hurst et al. (1998)).

Due to the extreme contrast in the number of rotor bars, slot harmonics are of higher frequency than the side bands of the supply frequency(Cameron et al. (1986)), which make it relatively easier to separate it from the operating frequency. However, the magnitude of slot harmonics is still very small, even submerged by noise, making it challenging to extract from noisy measurements. Existing techniques that specialize in extracting that sideband may be not suitable for detecting harmonics along with the noise.

To address these issues, this paper proposes a technique to extract anomalous signals by a novel signal processing technique to extract fault signatures effectively. The contributions of this paper are as follows.

(1) We propose a weighted-sparsity-driven and graph-model-based method to extract motor fault signatures in the time-frequency domain.
(2) We formulate the fault signature extraction problem as a regularized optimization problem by imposing sparsity of fault signatures in the frequency domain and smoothness of fault signature in the time-domain, and putting frequency-dependent weight on the frequency spectrum, and then solve the problem us-

ing an alternating direction method of multipliers (ADMM) algorithm.

(3) We demonstrate with experimental results that not only high-frequency slot harmonics but also low-frequency sidebands of the supply frequency can be extracted as fault signatures simultaneously using our proposed method.

2. SLOT HARMONIC EXTRACTION

2.1 Physical model of slot harmonics

Theoretical studies have been conducted to formulate slot harmonics(Cameron et al. (1986), Henao et al. (2005)). Slot harmonics are induced in the stator current when rotor bars cross through the magnetic field generated by the stator windings. The slot harmonics can be expressed by the following equation(Vas (1992))

$$f_h = [(kR \pm n_d)\frac{(1-s)}{p} \pm \nu]f_s, \tag{1}$$

where k is an integer number, R is the number of rotor bar, n_d is the order of dynamic eccentricity, s is the motor slip, p is the number of pole pair, ν is the order of static eccentricity, and f_s is the operating frequency.

When $n_d = 0$, (1) represents the frequency of static eccentricity. When a static eccentricity fault is present, the magnitude of the slot harmonics increases. When $n_d = 1, 2, \ldots,$ it represents the frequency of dynamic eccentricity. When dynamic eccentricity exists, it will appear as a sideband frequency of slot harmonics.

2.2 Weighted sparsity-driven and graph-based model

To process non-stationary signals, the short-time Fourier transform (STFT) is used, representing the signal in the time-frequency domain. Signals are divided into short sections via overlapped time windows, and each section's frequency spectrum is analyzed using the fast Fourier transform (FFT). This process, applied to stator current in single or three-phase systems, produces a spectrogram matrix $\mathbf{Y}$, showing the frequency spectrum of each signal section. The matrix's rows correspond to fixed frequencies, with the frequency range limited to $[0, F_s/2]$ to avoid redundancy, where F_s is the sampling rate. Associated with the m^{th} node (time window) of the graph, a N_f-dimensional frequency spectrum vector $\mathbf{Y}_m \in C^{N_f}$ is achieved by analyzing the time-domain measurements $\mathbf{y}_m \in R^{2N_f}$ via Fourier transform (FT) or other methods such as minimum-variance-based spectral analysis Liu et al. (2022) for better denoising performance. Let

$$\mathbf{Y}_m = \mathbf{X}_m + \mathbf{N}_m, \text{ for } m = 1, \ldots, M, \tag{2}$$

where $\mathbf{X} = [\mathbf{X}_1, \mathbf{X}_2, \cdots, \mathbf{X}_M]$ represents the denoised spectrogram and $\mathbf{N}_m$ is signal noise. Due to variable operating speed and load, the fault signature frequency varies, appearing as a curve in the spectrogram matrix.

To explore the data structure of $\mathbf{X}$, we have prior knowledge that $\mathbf{X}$ includes only a few number of frequency components. When the motor is in ideal healthy condition, $\mathbf{X}$ only includes the operating frequency component. If there is a fault, extra frequency components such as slot harmonics and fault frequency components will be introduced to $\mathbf{X}$. In both cases, $\mathbf{X}$ is sparse in the frequency domain. Therefore, we can impose sparsity on $\mathbf{X}$. Considering the harmonic magnitude decreases with the increase of frequency, a weighted sparsity regularizer is considered for recovering the sparse components, with weights related to the frequency.

To further explore the data structure of $\mathbf{X}$ and motivated by recent advancements in graph-model based signal denoising techniques (Chen et al. (2014); Liu et al. (2020): Liu et al. (2023)), we model the denoised spectra measurements on a graph $G = (\mathbf{V}, \mathbf{A})$, where $\mathbf{V} = \{v_1, ..., v_m, ..., v_M\}$ is the set of nodes, represented by sequential moving time windows. The spectrum $\mathbf{X}_m$ is the measurement at node v_m. $\mathbf{A} \in R^{M\times M}$ is the graph shift, or a weighted adjacency matrix that represents the pairwise proximity between nodes, which can be estimated using the STFT frequency spectra as

$$A_{i,j} = \frac{|\mathbf{Y}_i^H \mathbf{Y}_j|}{\sqrt{\mathbf{Y}_i^H \mathbf{Y}_i}\sqrt{\mathbf{Y}_j^H \mathbf{Y}_j}}, \text{ for } |i-j| < d, \tag{3}$$

where the superscript H indicates the matrix Hermitian transpose, d is the maximal distance of connected neighborhood nodes in the graph. We formulate the harmonic extraction problem as a regularized optimization problem as

$$\min_{\mathbf{X}} \sum_{m=1}^{M} \frac{1}{2} \|\mathbf{X}_m - \mathbf{Y}_m\|_2^2 + \lambda R_1(\mathbf{X}) + \beta R_2(\mathbf{X}). \tag{4}$$

Here $R_1(\mathbf{X})$ and $R_2(\mathbf{X})$ are regularization terms. $R_1(\mathbf{X})$ enforces the sparsity of the graph signal by utilizing weighted L_1 norm as

$$R_1(\mathbf{X}) = \sum_{m=1}^{M} |\mathbf{W} \odot \mathbf{X}_m|_1 = \sum_{m=1}^{M} |\text{diag}(\mathbf{W})\mathbf{X}_m|_1, \tag{5}$$

where $\mathbf{W}$ is a frequency dependent one-dimensional weight vector, and $\odot$ represents element-wise product. By weighting the frequency spectrum $\mathbf{X}_m$, the low-magnitude harmonic frequency component can be well detected.

$R_2(\mathbf{X})$ encourages the smoothness of graph signals, meaning that adjacent nodes are expected to have similar fault signatures in the frequency domain, which can be formulated as

$$R_2(\mathbf{X}) = \frac{1}{2}\|\mathbf{X} - \bar{\mathbf{A}}\mathbf{X}\|_F^2. \tag{6}$$

where $\bar{\mathbf{A}}$ is a normalized graph shift matrix whose entries are computed as $\bar{A}_{i,j} = \frac{A_{i,j}}{\sum_j A_{i,j}}$ to ensure that the sum of each row of $\bar{\mathbf{A}}$ equals to 1; and the subscript F denotes the Frobenius norm.

2.3 Weight design

This weight vector $\mathbf{W}$ in (5) is designed to be frequency dependent, with the magnitude of the weights decreasing as the frequency increases. To explore the magnitude variation of the stator current with respect to the frequency, we study the physical model of induction machines. Fig. 1 shows an equivalent circuit of an induction motor when we ignore the motor slip, which circuit is similar to that of a transformer(Kron (1951)).

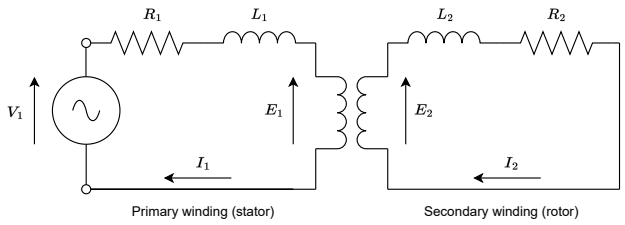

Fig. 1. Equivalent circuit of induction motor. The circuit is similar to that of a transformer, where the stator is considered the primary and the rotor is the secondary.

Assume a simple structure with a stator as the primary and a rotor as the secondary, each containing a coil and a resistor, where V_1 is the applied voltage, L, R, I, and E are reactance, resistance, current, and induced voltage, respectively. The footnote 1 represents the primary side, and the footnote 2 represents the secondary side. When three-phase alternating voltage is applied to the primary side, a stator current is generated, which is inversely proportional to the equivalent primary impedance. Any fault occurred in the motor will be reflected in the equivalent impedance, and consequently in the stator current. Since the excitation current is very small compared to the stator current, the impedance of the stator on the primary side can be expressed by

$$|Z|_1 = \sqrt{{C_R}^2 R_1^2 + {C_L}^2 \omega^2 L_1^2} + |Z|_2', \tag{7}$$

where ω is the angular frequency, and C_R and C_L are the coefficients of inductance and resistance, and $|Z|_2'$ is the equivalent impendance of the secondary winding. The magnitude of the current can be obtained by

$$\begin{aligned} |I| &= \frac{|V|}{|Z|_1} \\ &= \frac{|V|}{2\pi L_1 C_L \sqrt{\left(\frac{C_R}{2\pi L_1 C_L}\right)^2 R_1^2 + f^2} + |Z|_2'} \\ &\approx |V|\left(\frac{C_1}{\sqrt{C_2 + f^2}} + C_0\right), \end{aligned} \tag{8}$$

where I is the stator current, V is the supply voltage, and C_0, C_1, and C_2 are constants related to motor parameters. In induction motors, these constants are closed tied by several factors such as skin effect, saturation, and slip between synchronous speed and rotor speed.

Fig. 2 shows the admittance with respect to frequency when $C_0 = 1.5$, $C_1 = 0.25$, and $C_2 = 0.02$, where the admittance decreases monotonically with frequency.

Since the current is proportional to the admittance, the envelop of current spectrum also decreases with frequency. By setting the admittance as a weight vector, small-magnitude harmonics at higher frequency band can be extracted effectively. The ith entry of the weight vector can be calculated as

$$\mathbf{W}(i) = \frac{C_1}{\sqrt{C_2 + f_i^2}} + C_0, \quad \text{for } i = 1, ..., N_f, \tag{9}$$

where N_f is the total number of discrete frequency considered in the spectrum and f_i represent the i^{th} discrete frequency.

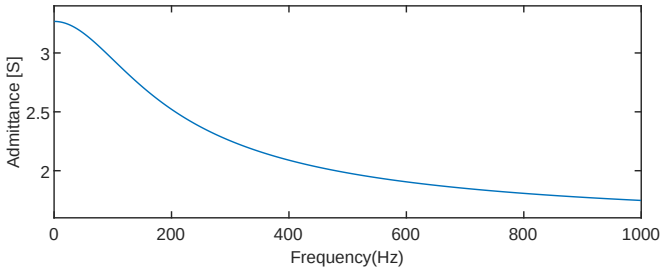

Fig. 2. Admittance of stator winding. The admittance decreases monotonically with frequency, resulting decreased harmonic magnitude with respect to frequency.

2.4 Algorithm

To solve the optimization problem in (4), we utilize the augmented Lagrangian approach and implement the alternating direction method of multipliers (ADMM) for its solution Boyd et al. (2011), and use the following unconstrained objective function

$$\begin{aligned} \min_{\mathbf{X},\mathbf{U}} \sum_{m=1}^{M} \frac{1}{2} \|\mathbf{X}_m - \mathbf{Y}_m\|_2^2 + \lambda \sum_{m=1}^{M} |\mathbf{Z}_m|_1 + \frac{\beta}{2} \|\mathbf{X} - \bar{\mathbf{A}}\mathbf{X}\|_F^2 \\ + \frac{\rho}{2} \|\text{diag}(\mathbf{W})\mathbf{X} - \mathbf{Z} + \mathbf{U}\|_F^2. \end{aligned} \tag{10}$$

The entire process of extracting harmonic signatures is summarized in Algorithm 1, where $\mathbf{I}$ denotes an identity matrix and $S_\alpha(z)$ represents a soft-thresholding function Donoho (1995)

$$S_\alpha(z) = \max\left(|z| - \alpha, 0\right) \frac{z}{|z|}. \tag{11}$$

Algorithm 1 ADMM solution of the proposed method

Input $\mathbf{Y}$, $\bar{\mathbf{A}}$, β, ρ, N_f
  $k \leftarrow 1$
  $\mathbf{U}^{(0)} \leftarrow \mathbf{0}$, $\mathbf{X}^{(0)} \leftarrow \mathbf{1}$, $\mathbf{Z}^{(0)} \leftarrow \mathbf{W} \odot \mathbf{X}^{(0)}$
  while $\frac{\|\text{diag}(\mathbf{W})\mathbf{X}^{(k)} - \mathbf{Z}^{(k)}\|}{\|\mathbf{Z}^{(k)}\|} \geq 10^{-6}$ **do**
    For $i = 1, ..., N_f$
      $\mathbf{X}^{(k)}(i) \leftarrow [(\rho\mathbf{W}(i)^2 + 1)\mathbf{I} + \beta(\mathbf{I} - \bar{\mathbf{A}})^T(\mathbf{I} - \bar{\mathbf{A}})]^{-1}$
        $[\mathbf{Y}(i) + \rho\mathbf{W}(i)(\mathbf{Z}^{(k-1)}(i) - \mathbf{U}^{(k-1)}(i))]$,
    End
    $\mathbf{Z}^k \leftarrow S_{\lambda/\rho}(\text{diag}(\mathbf{W})\mathbf{X}^{(k)} + \mathbf{U}^{(k-1)})$,
    $\mathbf{U}^k \leftarrow \mathbf{U}^{k-1} + \text{diag}(\mathbf{W})\mathbf{X}^k - \mathbf{Z}^k$,
  end while
Output $\hat{\mathbf{X}} = \mathbf{X}^{(k)}$

3. EXPERIMENTS

3.1 Experiment setup

To demonstrate the effectiveness of our proposed method, experiments were conducted on a 1 HP three-phase squirrel-cage induction motor driven by a three-phase inverter, as depicted in Fig. 3(a). A servo-motor was precisely aligned on the shaft of the induction motor to serve as an adjustable load, allowing for precise manipulation of its speed and torque during the experiment. The stator

currents of the three-phase motor are collected through three current sensors and subsequently stored via a computer interface for detailed analysis.

In our comparative analysis, two identically specified rotors were used. We intentionally created a broken-bar defect in one of them by drilling into a rotor bar. Pictures of both the healthy and the faulty rotors are displayed in Fig. 3(b). In the experiments, we manually adjust the load torque to mimic practical varying load operations.

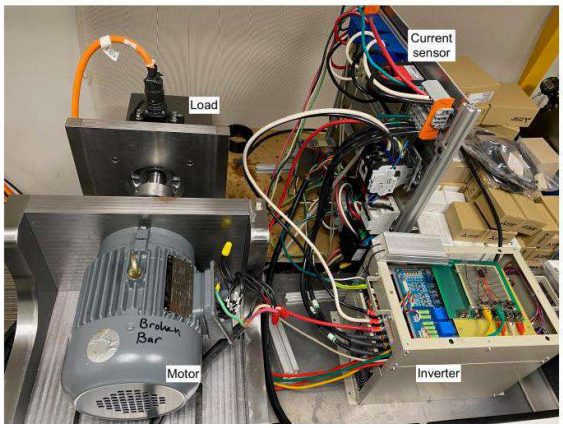

(a) Configuration of experimental Setup. The induction motor has 32 stator slots, 28 rotor bars, and 2 pole pairs.

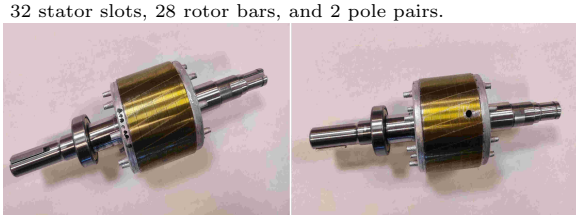

(b) The left figure shows a healthy rotor and the right figure shows a broken-bar rotor.

Fig. 3. Experimental setup using healthy and faulty rotors.

3.2 Experimental results

In this experiment, the evaluation was performed on data from an induction motor operating under varying load conditions. Fig. 4(a) shows the data in the time domain and Fig. 4(b) shows the data in the frequency domain of 0-1000 Hz. From Fig. 4(a) we can see that the stator current amplitude changes with time due to load variation. As a result, the corresponding fault frequency (harmonics at around 800Hz) also changes as indicated in Fig. 4(b).

To evaluate the proposed method, we compare it with three existing methods, which are (a) short-time Fourier transform (STFT), (b) minimum variance-based spectral analysis (MV), and (c) sparsity-driven graph model-based method (Graph-based)(Liu et al. (2023)). For all experiments, we use time-domain stator current measurements of 53s. For fair comparison, the same sliding time window is used with a length of 2.5s and an overlap of 0.5s from window to window. Other hyper-parameters are listed in Table 1.

Fig. 5 shows the frequency analysis results for a healthy rotor bar. Fig. 5(a) shows STFT, Fig. 5(b) shows MV, Fig. 5(c) shows graph-based, and Fig. 5(d) shows the

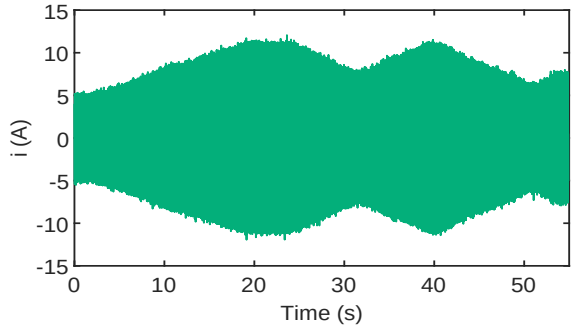

(a) Time domain

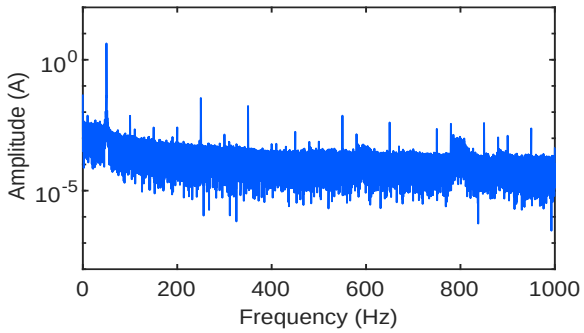

(b) Frequency domain

Fig. 4. Stator current of varying frequency operation in (a) time-domain and (b) frequency-domain using Fourier transform.

Table 1. Hyper parameters

Parameter	β	ρ	λ	C_0	C_1	C_2
Value	0.01	0.02	0.03	1.5	0.25	0.02

proposed method. We consider frequency range from 0 to 100Hz which covers the sideband frequency range and current magnitude from -50dB to 20dB. The magnitude of the signal at the driving frequency of 50Hz is 10dB, but the slot harmonics are about -60dB. We observe that for STFT spectrum, there exists a large amount of noise besides the operating frequency. The minimum variance method is able to suppress the noise and the graph-based method suppressed more. While our proposed method clearly removed all noise in the spectral analysis. Further investigation shows that our proposed method removes noise over a wide frequency range as indicated in the following results.

Fig. 6 shows an zoom-in view from 400Hz to 1000Hz. To improve the visual contrast, the dynamic range of the color bar is set from -75dB to -50dB. Comparing Fig. 6(a) to Fig. 6(d), we can see that the proposed method is able to extract harmonics effectively. Fig. 6(e) is a plot of theoretical result according to (1). Comparing with this Fig. 6(d), it can be seen that the extraction results are theoretically supported.

Fig. 7 shows the frequency analysis results of stator current with a broken-rotor-bar fault. Similar to Fig. 5, Fig. 7(a) is STFT, Fig. 7(b) is MV, Fig. 7(c) is graph-based, and Fig. 7(d) is the proposed method, with the same settings as Fig. 5. It can be seen that the proposed method is able to clearly extract driving signal as well as the results for a healthy rotor bar in Fig. 5. Furthermore, the

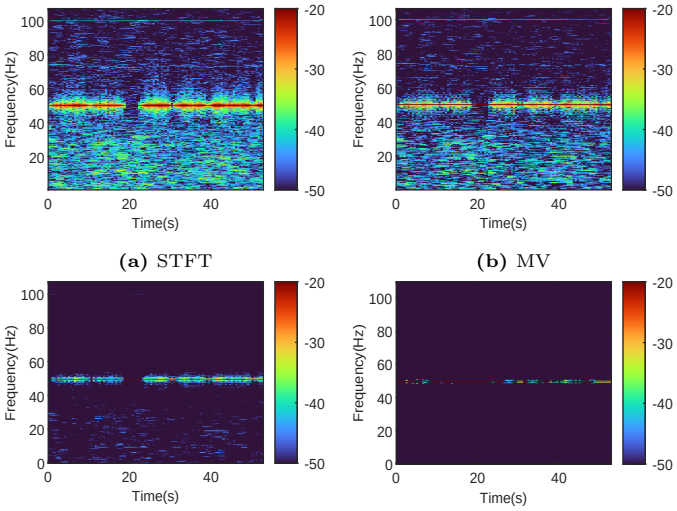

(a) STFT **(b)** MV

(c) Graph-based **(d)** Proposed Method

Fig. 5. Comparison of denoising results on healthy motor current data using 5(a) STFT, 5(b) MV, 5(c) Graph-based, and 5(d) Proposed method, respectively. It can be observed that the proposed method effectively reduce noise in the range of 0 - 100 Hz, and extract driving frequency signature at 50Hz.

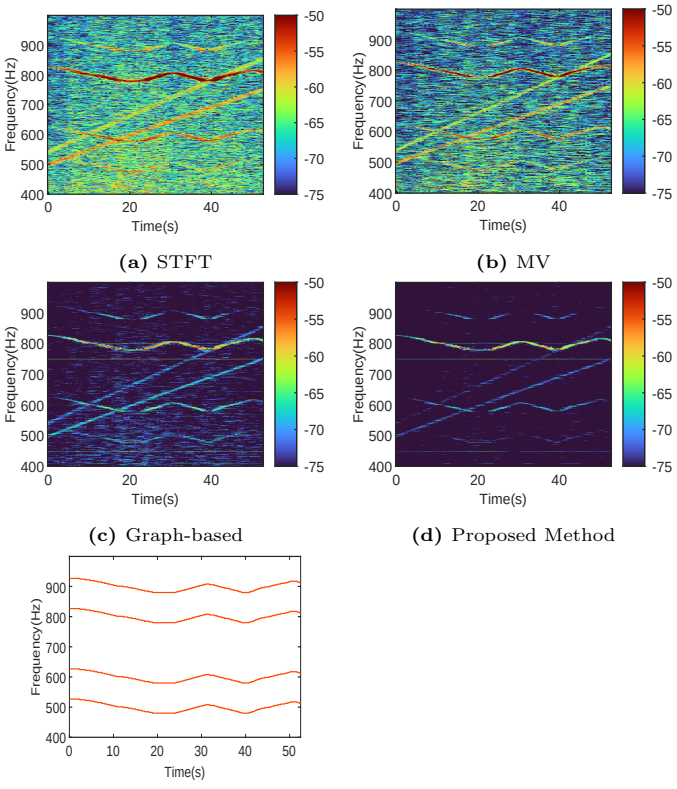

(a) STFT **(b)** MV

(c) Graph-based **(d)** Proposed Method

(e) Slot harmonics via (1)

Fig. 6. Comparison of denoising techniques in the range of 400 - 1000Hz. Four harmonics are identified, $\nu = +5, +3, -1, -3$ from top to bottom respectively. The extracted feature signal (6(d)) is found to be consistent with the theoretical equation (6(e)).

sideband signal, which appears around 50Hz due to rotor bar damage, is also extracted. Similarly, a zoomed-in view of Fig. 8 is shown in the frequency range 400Hz to 1000Hz. Comparing with the theoretical result plotted in Fig. 8(e), we can observe that the extracted slot harmonics agree with the theoretical result very well.

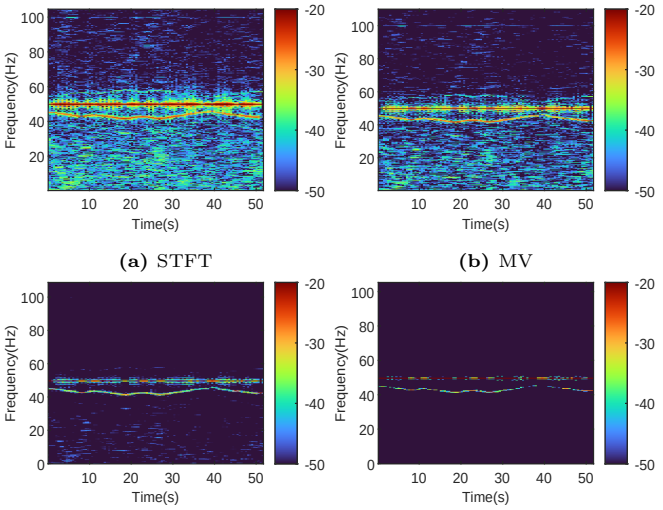

(a) STFT **(b)** MV

(c) Graph-based **(d)** Proposed method

Fig. 7. Comparison of denoising results on stator current of a motor with broken-bar fault using 7(a) STFT, 7(b) MV, 7(c) Graph-based, and 7(d) Proposed method, respectively. The proposed method can successfully extract the low frequency broken-bar fault signature around 50Hz operating frequency.

The results from Figs. 5-8 show that the proposed method is able to extract low frequency fault signatures and high frequency harmonics more effectively than existing methods.

4. CONCLUSION

This study presented a novel weighted sparsity-driven and graph-model based approach to extracting harmonic signatures from noisy stator current of induction motor. Our method demonstrated superior performance in identifying slot harmonics and sidebands of the driving frequency, outperforming traditional techniques like STFT and MV-based spectral analysis. These advancements significantly enhance fault detection capabilities, which is crucial for predictive maintenance in various industrial applications. The effectiveness of proposed method in noise reduction and accurate harmonic extraction shows great potentials for industrial applications.

REFERENCES

Bonet-Jara, J., Pons-Llinares, J., and Gyftakis, K.N. (2022). Comprehensive analysis of principal slot harmonics as reliable indicators for early detection of inter-turn faults in induction motors of deep-well submersible pumps. *IEEE Transactions on Industrial Electronics*.

Boyd, S., Parikh, N., Chu, E., Peleato, B., Eckstein, J., et al. (2011). Distributed optimization and statistical learning via the alternating direction method of multipliers. *Foundations and Trends® in Machine learning*, 3(1), 1–122.

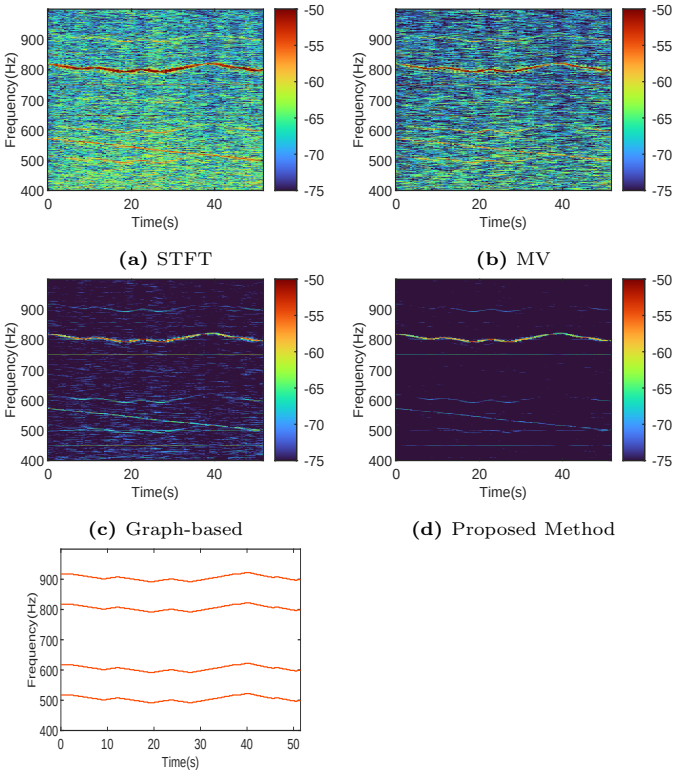

(a) STFT **(b)** MV **(c)** Graph-based **(d)** Proposed Method

(e) Slot harmonics via (1)

Fig. 8. Comparison of denoising techniques in the range of 400 - 1000Hz. Similar to Fig. 6, four harmonics are identified, corresponding to $\nu = +5, +3, -1, -3$ in (1) from top to bottom respectively. While the load fluctuation is different from that in Fig. 6, the the extracted harmonics shown in 8(d) is still consistent with the theoretical result shown in 8(e).

Cameron, J., Thomson, W., and Dow, A. (1986). Vibration and current monitoring for detecting airgap eccentricity in large induction motors. In *IEE Proceedings B (Electric Power Applications)*, volume 133, 155–163. IET.

Chen, S., Sandryhaila, A., Moura, J.M., and Kovacevic, J. (2014). Signal denoising on graphs via graph filtering. In *2014 IEEE Global Conference on Signal and Information Processing (GlobalSIP)*, 872–876. IEEE.

Donoho, D.L. (1995). De-noising by soft-thresholding: Ieee transactions on information theory.

Faiz, J. and Moosavi, S. (2016). Eccentricity fault detection–from induction machines to dfig—a review. *Renewable and Sustainable Energy Reviews*, 55, 169–179.

Henao, H., Razik, H., and Capolino, G.A. (2005). Analytical approach of the stator current frequency harmonics computation for detection of induction machine rotor faults. *IEEE Transactions on Industry Applications*, 41(3), 801–807.

Hurst, K.D., Habetler, T.G., Griva, G., and Profumo, F. (1998). Zero-speed tacholess im torque control: Simply a matter of stator voltage integration. *IEEE Transactions on Industry Applications*, 34(4), 790–795.

Kron, G. (1951). *Equivalent circuits of electric machinery.*

Liu, D., Chen, S., and Boufounos, P.T. (2020). Graph-based array signal denoising for perturbed synthetic aperture radar. In *IGARSS 2020-2020 IEEE International Geoscience and Remote Sensing Symposium*, 1881–1884. IEEE.

Liu, D., Inoue, H., and Kanemaru, M. (2022). Robust motor current signature analysis (mcsa)-based fault detection under varying operating conditions. In *2022 25th International Conference on Electrical Machines and Systems (ICEMS)*, 1–5. IEEE.

Liu, D., Varatharajan, A., and Goldsmith, A. (2023). Extracting broken-rotor-bar fault signature of varying-speed induction motors. In *Prcoceedings of the Asia Pacific Conference of the PHM Society 2023*, volume 4.

Pillay, P. and Xu, Z. (1996). Motor current signature analysis. In *IAS'96. Conference Record of the 1996 IEEE Industry Applications Conference Thirty-First IAS Annual Meeting*, volume 1, 587–594. IEEE.

Thomson, W.T. and Fenger, M. (2001). Current signature analysis to detect induction motor faults. *IEEE Industry Applications Magazine*, 7(4), 26–34.

Vas, P. (1992). *Parameter estimation, condition monitoring, and diagnosis of electrical machines.* Oxford University Press.